Radiation hardness studies of neutron irradiated CMOS sensors fabricated in the ams H18 high voltage process

2016 JINST 11 P02016

(http://iopscience.iop.org/1748-0221/11/02/P02016)

Published by IOP Publishing for Sissa Medialab

Received: *November 10, 2015*
Revised: *January 14, 2016*
Accepted: *January 29, 2016*
Published: *February 26, 2016*

2016 JINST 11 P02016

Radiation hardness studies of neutron irradiated CMOS sensors fabricated in the ams H18 high voltage process

M. Fernández García,[a,1] **C. Gallrapp,**[b] **M. Moll**[b] **and D. Muenstermann**[c,d]

[a] *Instituto de Física de Cantabria (CSIC-UC), Avda. los Castros s/n, E-39005 Santander, Spain*
[b] *CERN, Organisation européenne pour la recherche nucléaire, CH-1211 Genève 23, Switzerland*
[c] *Un. de Genève, DPNC, Quai Ernest-Ansermet 24, 1205 Genève, Switzerland*
[d] *Department of Physics, Lancaster University, Lancaster, LA1 4YB, U.K.*

E-mail: Marcos.Fernandez@cern.ch

Abstract: High voltage CMOS detectors (HVCMOSv3), fabricated in the ams H18 high voltage process, with a substrate resistivity of 10 Ω·cm were irradiated with neutrons up to a fluence of 2×10^{16} n_{eq}/cm^2 and characterized using edge-TCT. It was found that, within the measured fluence range, the active region and the collected charge reach a maximum at about 7×10^{15} n_{eq}/cm^2 to decrease to the level of the unirradiated detector after 2×10^{16} n_{eq}/cm^2.

Keywords: Radiation-hard detectors; Radiation damage to detector materials (solid state); Hybrid detectors; Radiation-hard electronics

[1] Corresponding author.

doi:10.1088/1748-0221/11/02/P02016

Contents

2016 JINST 11 P02016

1 Introduction

While the experiments at the Large Hadron Collider (LHC) are taking data, detector upgrades for its High Luminosity phase (HL-LHC) are being planned. With increasing luminosity, the radiation damage will scale and thus extremely radiation tolerant sensors — up to $O(10^{16}$ $n_{eq}/cm^2)$ [1, 2] — are required for the trackers. At the same time, the areas to instrument are very large ($O(100$ $m^2)$) and thus cost effective technologies have to be explored to keep the cost for the upgrades affordable.

To a certain extent, the cost associated with radiation-tolerant silicon detectors is due to the fact that highly specialized foundries have been producing them using small wafer sizes (4″ and 6″). Silicon sensors produced using CMOS processes are very cost effective when produced in large quantities. They will however not be radiation-tolerant if they rely on charge diffusion rather than collection by drift. The key idea to manufacture large quantities of radiation-hard sensors using industry standard CMOS processes is therefore the application of a drift field. While there had been earlier studies using an adopted process and dedicated base materials [3], this was first explored in standard foundries using so-called High-Voltage CMOS (HV-CMOS) processes [4]. In industrial applications, this technology is used to switch high voltages (up to 60 V) directly using an integrated circuit without the need for an external relay.

1.1 HV-CMOS sensors

One of the features of HV-CMOS processes is the existence of a deep N-well (DNW) in a moderately p-doped bulk which is necessary to insulate the circuits from high voltages. Its depth of — depending on the process — few µm avoids that the depletion zone inside the well reaches the shallow n- and p-wells, which constitute the circuits that are embedded within the DNW (see figure 1 left). The DNW itself must also have a suitable doping profile that avoids too high electric fields at its edges which would cause impact ionization and thus breakdown.

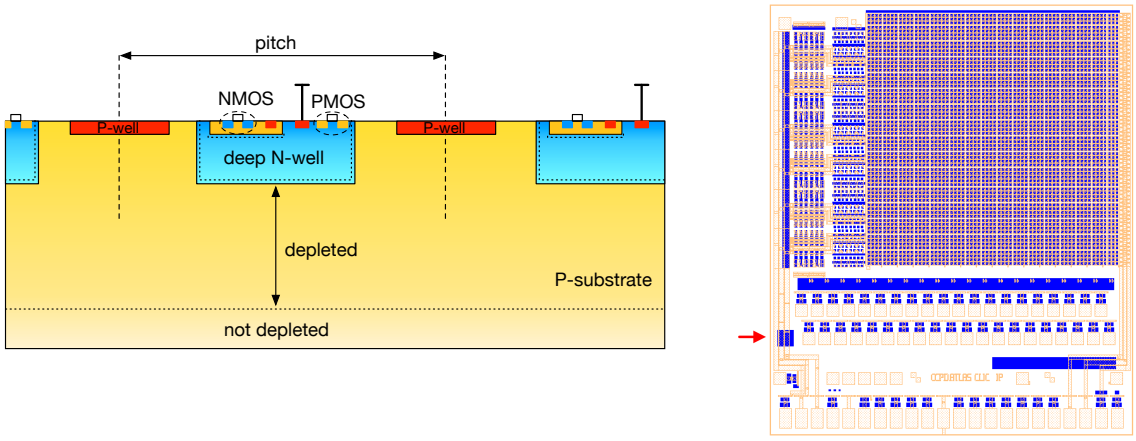

Figure 1. Left: schematic cross section of an HV-CMOS sensor. The deep N-well is the charge-collecting electrode and also contains additional CMOS circuits such as a preamplifier. Right: drawing of the CCDPv3 sensor used for this study. Visible are the top metal (brown) and the deep N-wells (blue). The passive diode used for the edge-TCT measurements is indicated by the red arrow.

In its most simple form, a matrix of DNWs could be used as a classical planar n^+-in-p pixel detector. However, the resistivity of the standard base material is only 10-20 $\Omega \cdot$cm leading to a calculated depletion depth of only about 10-15 µm for bias voltages of 80-150 V. Such thin layers of silicon would yield a (most probable) charge of only about 600 – 900 electrons for a vertically penetrating minimum ionizing particle (MIP), clearly a very challenging value for classical pixel readout chips with usual threshold settings of 2000 electrons or above.

Being produced in a CMOS process, in-pixel amplification is possible and can be used to increase the signal amplitude to a suitable level for a discriminator or directly for a readout chip. HVCMOS sensors can be read out coupling them directly to a readout chip, for instance the ATLAS FE-I4 [5]. We have tested in this work the *HV2FEI4* sensor also known as *Capacitively Coupled Pixel Detector* [4]. This sensor is being developed for use in the upgraded ATLAS detector at HL-LHC. As suggested by the name, readout can be provided by capacitive coupling to the chip using e.g. non-conductive glue. The in-pixel amplified output signal from the detector is large and fast enough to capacitively couple to the readout chip and not be distorted by the glue-filled gap in the signal path. The CCPD sensors (version 3) were built on a nominal 10 $\Omega \cdot$cm substrate. They contain a pixel matrix matching both the FE-I4 and ClicPix [6] readout chips with pixels between 25 and 33 µm pitch and test structures such as the passive 100×100 µm^2 diode highlighted in figure 1 right which was used in the measurements presented here.

1.2 The edge-TCT technique

In TCT (Transient Current Technique) charge carriers are created inside a detector and their movement is registered as an induced current on the electrodes. Injection of charge carriers can be done by using a radioactive source, an ion beam or a laser. By using fast electronics this induced current is time resolved and recorded. The measurements in this work employed a picosecond-pulsed laser [7] with a pulse duration and pulse rate of ~250 ps and 200 Hz, respectively. The wavelength is 1064 nm, where the absorption length of silicon allows photons to penetrate the full detector active volume.

2016 JINST 11 P02016

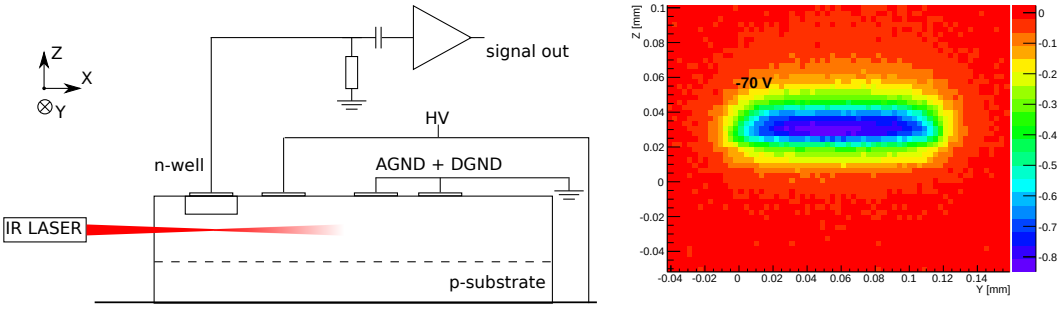

Figure 2. Left: laser incidence in edge-TCT for a HVCMOS test diode and biasing scheme. Right: 2D charge profile of an unirradiated detector. The charge integrated in 5 ns is displayed as a function of the laser beam position (Y, Z).

In edge-TCT [8], incidence is from the cutting edge of the detector (see figure 2 left). During the measurement, a collimated and focused laser beam is scanned across the edge of the sensor (using motorized 3D stages). By integrating the induced current over the collection time, it is possible to map the collected charge as a function of the position where the charge was generated. Figure 2 (right) shows such a charge map, where the beam has been scanned over the edge of the detector (YZ scan, figure 2 left). Once the sensor boundaries were identified, vertical scans (Z scans, normally done at the center of the detector, e.g. Y=0.06 mm in figure 2 right) are done at different voltages. This scan, shown in figure 3 left for several voltages, provides a depth profile of the depletion region in the detector. The width of the depleted region is calculated as the Full Width Half Maximum (FWHM) of these charge profiles.

For the measurements, a laser beam with gaussian propagation and width of σ_{laser} =10 µm was employed. The beam size and focusing position were calculated using the knife-edge technique [9] on a fully depleted 300 µm thick microstrip detector. For this characterization, the waist and focus are estimated from the width of collected charge profiles (Z scans) measured at different positions along the beam path (X direction). The focus is identified as the position where the width is minimum (see figure 3 right). Once the focus was found (for this example around position X=59 mm), the HVCMOS detector was placed in this position and the focus searched again around this point.

Spatial resolution of edge-TCT depends on the width of the laser. For depletion depths comparable or below σ_{laser} the measured charge profile width is dominated by the beam size. This is specially important for HVCMOS detectors on a low resistivity substrate, where the depletion depth is below 10 µm. Figure 4 (left) shows a simulation of the depleted thickness of a 10 Ω·cm diode, as it varies with voltage, and the reconstructed FWHM of the measured charge profile, as reconstructed using three different beam widths (σ_{laser} =1, 5, 10 µm). Clearly, the narrower the beam, the smaller the reconstruction error (difference between the simulated FWHM and the theoretical depletion width of a diode). This error is displayed in figure 4 (right) as a function of the measured FWHM, again for the three different beam sizes. Thus, as long as the real depleted thickness $w_p \geq 3.5\sigma_{\text{laser}}$ the beam width will not introduce an error in the calculation of the depth. This is the reason why a 300 µm thick detector was chosen to find the focus of the laser (beam size and focus are estimated from the width and position of charge profiles).

2016 JINST 11 P02016

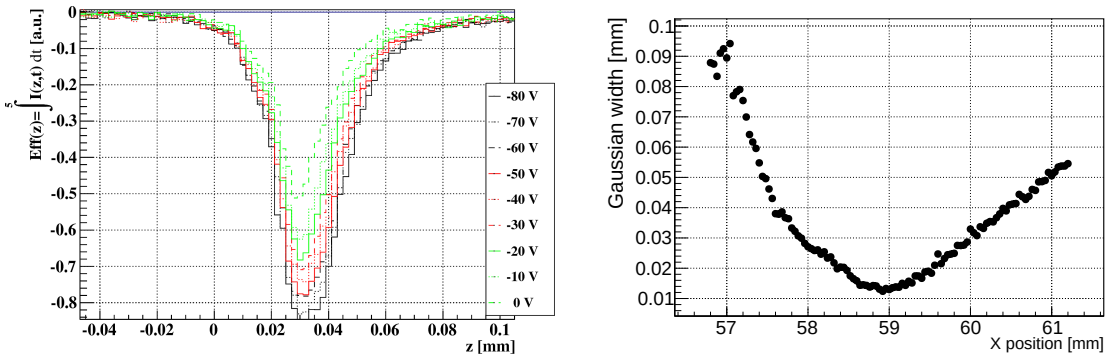

Figure 3. Left: a scan along the Z coordinate at the center of the detector for different bias voltages shows how the depleted area grows with voltage. Right: Gaussian width of the laser, as measured using a microstrip detector, versus the position of the sensor (motorized stage coordinates).

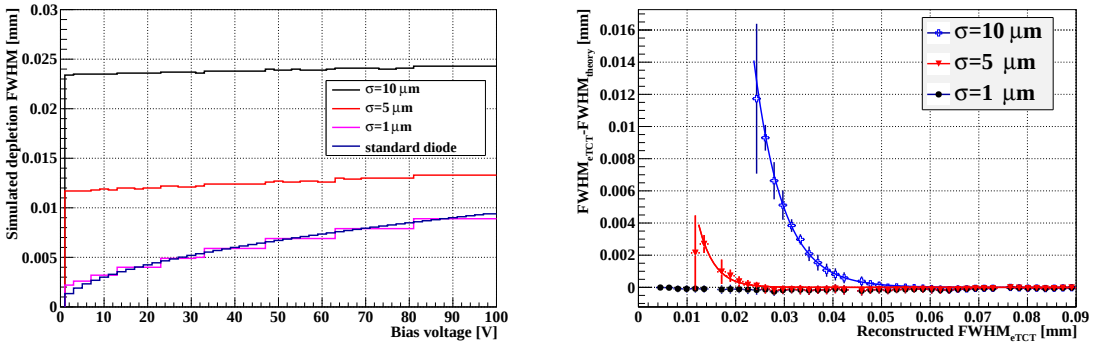

Figure 4. Left: depletion width for a 10 Ω·cm diode, as reconstructed by lasers of different waist. Right: difference between reconstructed FWHM (edge-TCT measurable quantity) and theoretical depletion width, as a function of the former, for different laser beam widths.

1.3 Samples, setup and measurements description

Three HVCMOS version 3 devices produced in the ams H18 process [10] were irradiated with neutrons at the TRIGA reactor in Ljubljana [11]. Fluence steps were 1×10^{15}, 7×10^{15} and 2×10^{16} n_{eq}/cm^2 respectively. One detector was not irradiated and used as a reference. Samples were kept at room temperature after irradiation and during storage for about 1 month. This paper presents measurements of an isolated diode, made by the junction of a Deep-N-Well (DNW) buried in a p-bulk (10 Ω·cm) located in one corner of the detector (see figure 1 right). The junction is separated from the matrix of pixels and does not contain any NMOS or PMOS electronics, but is otherwise identical to the N-wells used to isolate the electronics from the bulk in the rest of the detector. The diode was conceived as a test structure to study a basic n-on-p junction, using edge-TCT. After irradiation, the detectors were mounted on PCBs designed to match the 50 Ω impedance of the system (see figure 5). SMA connectors placed nearby allow for short wire bond connections. The analog signal picked from the DNW was connected to a 2 GHz current amplifier [12] after a 3

2016 JINST 11 P02016

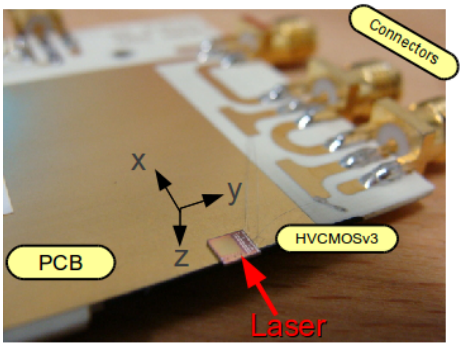

Figure 5. Picture of a HVCMOSv3 glued on the edge of a PCB. Wire bond connections to the three SMA connectors in the background corresponding to the schematic in figure 2 left.

m long delay line. The output of the amplifier was connected to a 2.5 GHz digital oscilloscope [13]. The rest of the chip pixel matrix was not powered and configured. Bias voltage was supplied via front-side implants (P-wells) surrounding every deep N-well, as suggested by the process design rules. In addition to the diode contact to GND, analog and digital grounds of the chip were shorted to a common GND, so that the leakage current from all other deep N-wells of the chip could bypass the edge-TCT diode (see figure 2 left). The detector was glued to the PCB using conductive glue. Breakdown voltage of the unirradiated detectors was reached slightly above 90 V.

The edge-TCT measurements of the HVCMOSv3 devices were performed in a new setup CERN-SSD TCT+ constructed by the Solid State Detector (SSD) team at CERN. This is a multi-purpose thermally controlled scanning TCT setup combining top, bottom and edge TCT in a single apparatus. Red (660 nm) and infrared (1060 nm) lasers are available for vertical TCT, while edge-TCT employs infrared. The samples to be measured are bonded to a PCB which is then placed on a copper sample support, providing cooling. The support is connected to a 3-axis movable platform to position the sample in the laser focus and perform the scan. The system is fully automatic and controlled by a LabView based control software. In particular, light injection direction is automatically selected by a system of optical shutters. Different parameters can be scanned to characterize the device under test: position (3D), temperature (T=−20 up to 60 °C), bias voltage or laser power. Combined scans of different parameters are also possible. To improve RF shielding, the setup is enclosed in a Faraday Cage [14], shielded coaxial cables are used everywhere, connectors are SMA type for high frequency operation.

For this measurement campaign, each detector was measured at three temperatures (-20, 0, 20 °C). For each temperature a YZ edge scan was performed (figure 2) with 3 µm resolution at three selected voltages (-70, -50, -30 V). Once the boundaries of the diode were found, three voltage scans (ZV scans, where V stands for bias voltage) were taken in the central part of the diode. In these voltage scans, the full depth of the detector is scanned with a spatial resolution of 2 µm at a fixed voltage. Then the voltage is ramped and the scan repeated. This kind of scan allows to evaluate the evolution of the depletion region with the bias voltage. The laser power was constantly monitored beam-splitting 10% of the light into a control branch ending on a commercial photodiode [15]. The laser output was measured to be stable within 1% for a period of two weeks.

2016 JINST 11 P02016

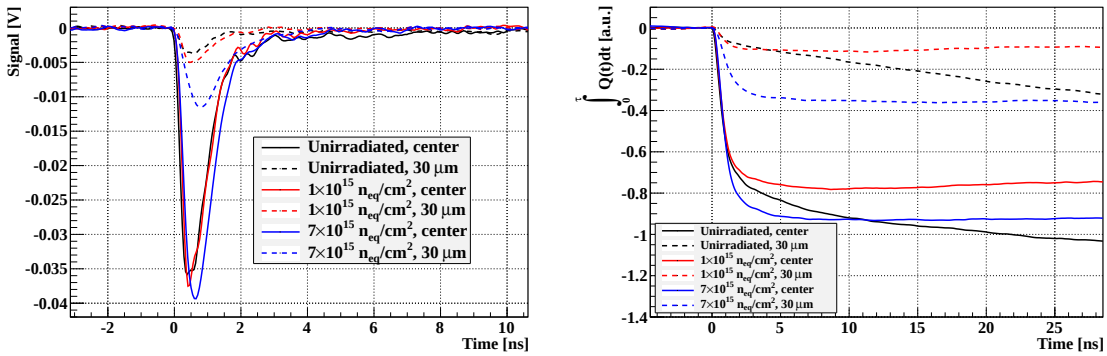

Figure 6. Left: time resolved transient current in the center of the depletion width, and 30 µm below, shown for two different fluences. The beginning of the pulse has been artificially moved to t=0. Right: running charge (accumulated charge as a function of integration time) for an unirradiated detector (black lines) and irradiated (red and blue). After irradiation charge is accumulated only by drift. For both plots, detector bias was −80 V at T=−20 °C.

2 Collected charge versus fluence

The picosecond infrared laser pulses generate photoinduced charge carriers at a specific depth with respect to the DNW (compare figure 2 left). These carriers drift inside the depleted bulk (or diffuse in the undepleted bulk) of the device and thus induce a current which can be measured. Figure 6 (left) shows an induced transient pulse measured with a non-irradiated HVCMOSv3 detector at −80 V and T=−20 °C. The duration of the signal (∼ 3 ns) is compatible with carrier movement by drift. Diffusion contributions to the signal are seemingly small compared to the signal induced by drift since no significant signal appears at longer times. They become only visible by integrating the signal. The waveforms shown in figure 6 (left) were recorded at the center of the depleted region (for the particular example of figure 2 right this would be (Y, Z)≈(0.05,0.03) mm) and 30 µm below this point, towards the bulk (Z≈0.06 mm). For comparison, we include in figure 6 (left) transients of another detectors irradiated to 1×10^{15} n_{eq}/cm^2 and 7×10^{15} n_{eq}/cm^2.

To unveil the contribution from diffusing charges to the measured signal, the accumulated charge as a function of integration time (running charge) in figure 6 (right) is evaluated. For an unirradiated detector, when injecting the laser at the center of the depleted region, the accumulated charge rises fast (as expected from drifting charge carriers) and then keeps on accumulating slowly (diffusion contribution). If the injection is done ∼30 µm below the center, the charge grows much slower and continuously. This shows that for the unirradiated detector, the depletion depth at −80 V is smaller than 30 µm. The slowly increasing contribution is due to charge carriers diffusing in the undepleted bulk and eventually entering the depleted region. For the irradiated detectors (shown for 1×10^{15} n_{eq}/cm^2 and 7×10^{15} n_{eq}/cm^2), the picture is very different. In both cases (center and off-centered incidence) the collected charge stops increasing after few nanoseconds. This is a clear sign that the diffusion component of the signal is suppressed by radiation induced trapping centers. Since charge is collected by drift 30 µm below the center of the diode, it can be assumed that the bulk at this fluence is depleted further than in the unirradiated detector.

2016 JINST 11 P02016

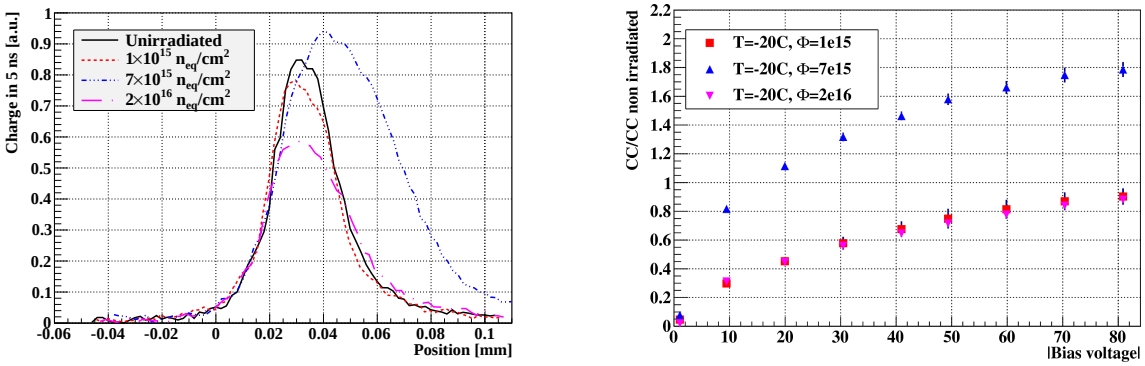

Figure 7. Left: collected charge (in 5 ns, T=-20 °C, −80 V bias) profiles for different fluences. Right: collected charge (in 5 ns, integrated over 90 µm depth, T=−20 °C) of irradiated detectors versus bias voltage referred to the collected charge of the unirradiated sample. Note the overlap of the data for the 1 ×10^{15} and 2×10^{16} samples.

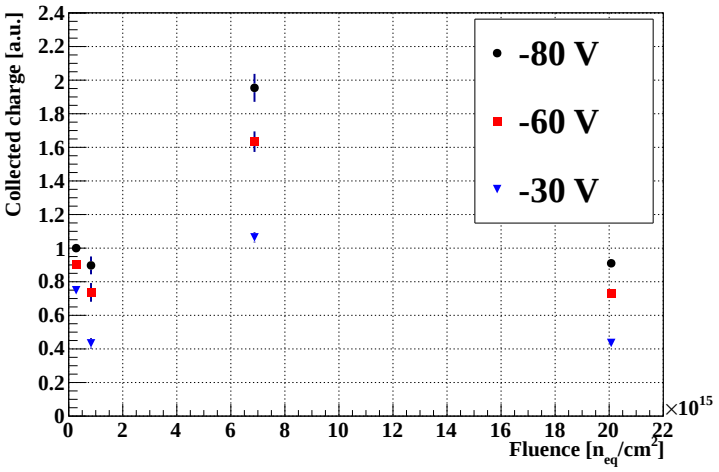

Figure 8. Collected charge (over 5 ns and extended 90 µm inside the bulk, T=−20 °C) versus fluence for 3 bias voltages. The charge is displayed in arbitrary units for the same laser power.

Figure 7 (left) shows charge profiles (Z scans) of an unirradiated detector, compared to profiles measured on irradiated detectors. All the profiles have been taken at the center of the depleted region. The charge in this plot was calculated as the integral of the waveform currents in the time interval between 0 and 5 ns. The 0 value in position for this plot has been chosen so that the rising edge of the charge distributions coincide. Measurements were taken at T=−20 °C and −80 V. The figure clearly shows how the profile width at half maximum after 1×10^{15} n_{eq}/cm^2 is similar to the unirradiated sample having however a smaller amplitude. After 7×10^{15} n_{eq}/cm^2 the charge profile is wider (i.e. the active region extends deeper into the bulk) and the amplitude is higher compared to the other fluences and even the non-irradiated sample. Finally, after 2×10^{16} n_{eq}/cm^2 the amplitude is the smallest and the width at half maximum is slightly bigger than that of the unirradiated sample.

2016 JINST 11 P02016

By integrating the charge profiles of figure 7 (left) from position Z=0 to Z=90 µm we can quantify the total collected charge in the diode, for each value of the bias voltage. The charge collected after irradiation is shown in figure 7 (right) as a function of the bias voltage and is normalized to the charge collected for the non-irradiated device for the same laser power and voltage. The collected charge after 5 ns, integrated over 90 µm at 1×10^{15} and 2×10^{16} n_{eq}/cm^2 turns out to be the same. The ratio with respect to the unirradiated sample is almost 1 at −80 V for both fluences. For 7×10^{15} n_{eq}/cm^2, however, the total collected charge surpasses that of the unirradiated detector after few volts and almost doubles at −80 V.

Figure 8 shows the total integrated charge (in 5 ns, over 90 µm, different detectors) as function of fluence for three different voltages, at T=−20 °C (not referenced to the unirradiated detector in this case). The total collected charge drops slightly after 1×10^{15} n_{eq}/cm^2, then rises again to reach a maximum at 7×10^{15} n_{eq}/cm^2 and finally decreases until 2×10^{16} n_{eq}/cm^2 to values smaller than for the non-irradiated detectors.

3 Depletion depth versus fluence

As already shown in figures 7 and 8, the depletion width and the collected charge at 7×10^{15} n_{eq}/cm^2 are bigger than before irradiation, pointing to a change in the effective doping concentration of the substrate or, in other words, to a change of resistivity across the bulk. Assuming a constant space charge density over the depleted volume, the effective space charge density can be calculated from the measured depletion width w_p using the expression:

$$w_p = \sqrt{\frac{2\epsilon_0\epsilon}{q N_{eff}}(V + V_b)} \tag{3.1}$$

where w_p is the depleted width, $\epsilon_0\epsilon$ the product of the vacuum and Si relative dielectric constants, q the electron charge, N_{eff} is the effective space charge density, V and V_b the bias and built-in voltages. To calculate N_{eff} we need to know the depletion depth at a specific bias voltage.

We can evaluate the impact of an error in the calculation of the depletion depth on N_{eff}, as the error made in quoting the measured FWHM as the real depleted thickness (see figure 4). By simple error propagation of equation (3.1) we arrive to the expression:

$$\sigma_{N\text{eff}} = \frac{4\epsilon_0\epsilon}{q}\frac{V + V_b}{w_p^3}\sigma_{w_p} \tag{3.2}$$

where σ_{w_p} is the difference between the measured and the real FWHM (σ_{w_p} is shown as ordinate of figure 4 right). A measurement error of 1 µm in the depletion depth w_p propagates to $\sigma_{N\text{eff}}$ ~4×10^{14} cm^{-3}, for $N_{\text{eff}} = 1.4 \times 10^{15}$ cm^{-3}. As seen in this figure, for σ_{laser} =10 µm the error can be above 10 µm. Therefore, for measured FWHM<$3.5\sigma_{\text{laser}}$ the calculated resistivity will have a non-negligible error that can be calculated using equation (3.2).

Figure 9 (left) shows the FWHM extracted from the measurements (at three different bias voltages, T=−20 °C) versus fluence. The reconstructed width is below 30 µm for the unirradiated and the 1×10^{15} n_{eq}/cm^2 irradiated detectors, then increases to almost 50 µm (7×10^{15} n_{eq}/cm^2) and drops back to 30 µm at 2×10^{16} n_{eq}/cm^2. According to the former explanation, calculated

2016 JINST 11 P02016

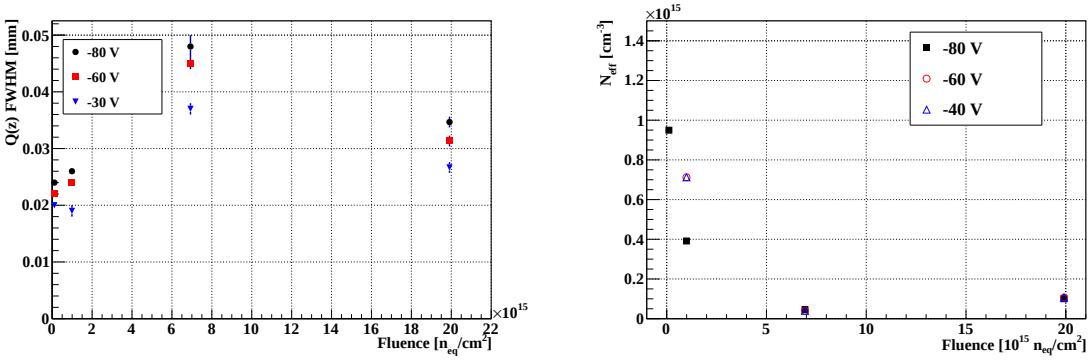

Figure 9. Left: measured depletion depth calculated as FWHM of charge profiles. Right: calculated effective doping concentration versus fluence.

widths above 35−40 µm should reflect the real depletion depth, while lower values will have a folded contribution of the laser beam width. Finally, figure 9 (right) shows the calculated doping concentration, as a function of fluence, using the depletion width corrected by the beam width. For this correction, figure 4 (right) is used. The reconstructed FWHM (abscissa) is used as input to calculate the error (ordinate) due to the beam width. The error value is subtracted from the reconstructed FWHM and the corrected FWHM used as w_p in equation (3.1). Using this correction, the calculated resistivity for the unirradiated detector at −80 V is 15 Ω·cm which is close to the nominal value of 10 Ω·cm provided by the producer. For lower bias voltages the calculated resistivity (unirradiated detector) is less accurate since the calculated depletion width is smaller and, according to figure 4 (right), the spread in the correction is bigger (see also equation (3.2)).

4 Discussion

Figure 9 (right) shows that the effective space charge decreases for fluences up to $\approx 7\times10^{15}$ n_{eq}/cm^2 having a positive impact on the depletion depth of the detector that extends deeper into the bulk for the same bias voltage. Nevertheless, comparing the collected charge for the unirradiated device and the device irradiated to 1×10^{15} n_{eq}/cm^2 we observe a decrease in the signal which is associated to the extinction of diffusion by trapping after irradiation. For even higher fluences the signal is rising again due to the increase of the active volume with the decrease of N_{eff}. This decrease in N_{eff} with rising fluence is usually described as “acceptor removal" as the overall negative space charge is decreasing. However, it is not obvious if this effect is caused by deactivation of the shallow acceptors or by compensation of the shallow dopants by positively charged deep defects. Our measurements are not able to distinguish one effect from the other. In any case, the effect leads to an increase of the active volume of the device and thus to an increase of the signal with rising fluence (see figure 8), an effect that is rarely observed in particle detectors. The signal reaches a maximum around 7×10^{15} n_{eq}/cm^2 and then starts to fall. This decrease is due to the combined effect of a shrinking active volume and increased trapping due to radiation induced defects.

2016 JINST 11 P02016

5 Summary and outlook

We measured four test diodes realized as deep-N-wells on low resistivity (10 Ω·cm) p-bulk produced in the ams H18 high voltage process. One of the detectors was not irradiated and therefore used as a reference. The other three were neutron irradiated to fluences of 1×10^{15}, 7×10^{15} and 2×10^{16} n_{eq}/cm^2.

For the first time observed, a detector irradiated to 7×10^{15} n_{eq}/cm^2 doubles the collected charge as measured with an IR laser beam, with respect to an unirradiated device. Even after 2×10^{16} n_{eq}/cm^2 the collected charge remained only slightly below the unirradiated reference.

After the lowest fluence irradiation, the contribution of diffusion to collected charge disappears, due to the long time constant of this process compared to trapping times. With further increased fluence, the depletion depth increases due to the acceptor removal effect. This leads to an increase of signal with increasing radiation damage. Even after the highest fluence of 2×10^{16} n_{eq}/cm^2 a signal corresponding to 90% of the unirradiated detector signal was observed at 80 V operational bias. A very promising result for the application of this technology in extremely high radiation environments.

Acknowledgments

This work was performed in the framework of CERN-RD50 collaboration. We would like to thank the team of the CERN DSF bonding lab (Florentina Manolescu, Ian McGill). We also thank our former summer students M. Brigida Brunetti and C. Weisser for first edge-TCT measurements on PCB prototypes. The research leading to these results has received funding from the European Commission under the FP7 Research Infrastructures project AIDA, grant agreement no. 262025. This work has been partially supported by the Spanish Ministry Economy and Competitiveness (MINECO) under grant number FPA2013-48387-C6-1-P.

References

[1] ATLAS collaboration, *Letter of intent for the phase-II upgrade of the ATLAS experiment*, CERN-LHCC-2012-022, CERN, Geneva Switzerland (2012).

[2] CMS collaboration, *Technical proposal for the phase-II upgrade of the CMS detector*, CERN-LHCC-2015-010, CERN, Geneva Switzerland (2015).

[3] P. Giubilato et al., *Monolithic pixels on moderate resistivity substrate and sparsifying readout architecture*, *Nucl. Instrum. Meth.* **A 731** (2013) 146.

[4] I. Peric, *A novel monolithic pixelated particle detector implemented in high-voltage CMOS technology*, *Nucl. Instrum. Meth.* **A 582** (2007) 876.

[5] M. Garcia-Sciveres et al., *The FE-I4 pixel readout integrated circuit*, *Nucl. Instrum. Meth.* **A 636** (2011) S155.

[6] P. Valerio et al., *A prototype hybrid pixel detector ASIC for the CLIC experiment*, 2014 *JINST* **9** C01012.

[7] PicoQuant, *Picosecond Pulsed Diode Laser*, LDH-P-C-1064 (IR), Rudower Chaussee 29, 12489 Berlin, Germany.

2016 JINST 11 P02016

[8] G. Kramberger et al., *Investigation of irradiated silicon detectors by edge-TCT*, *IEEE Trans. Nucl. Sci.* **57** (2010) 2294.

[9] J. Magnes et al., *Quantitative and qualitative study of Gaussian beam visualization techniques*, physics/0605102.

[10] ams AG, 0.18 *µm high-voltage CMOS process*, http://ams.com/eng/Products/Full-Service-Foundry/Process-Technology/High-Voltage-CMOS/0.18-m-HV-CMOS-process.

[11] M. Ravnik and R. Jeraj, *Research reactor benchmarks*, *Nucl. Sci. Eng.* **145** (2003) 145.

[12] CIVIDEC Instrumentation GmbH, *Cividec C2-TCT*, Schottengasse 3A/1/41, A-1010 Vienna, Austria.

[13] Agilent, *DSO9254A oscilloscope,* 2.5 *GHz,* 20 *GSa/s,* 4 *analog channels*.

[14] ETS Lindgren, type FI-27510, FI-27510 Eura, Finland.

[15] *DET01CFC* 1.2 *GHz InGaAs FC/PC-coupled photodetector,* 800–1700 *nm*, http://www.thorlabs.com.

2016 JINST 11 P02016